Electric Power Systems Research 213 (2022) 108730

Contents lists available at ScienceDirect

Electric Power Systems Research

journal homepage: www.elsevier.com/locate/epsr

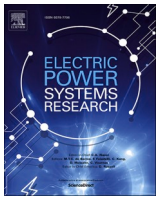

Potential use of space-based lightning detection in electric power systems

J. Montanyà [a,*], J.A. López [a], O. van der Velde [a], G. Solà [a], D. Romero [a], C. Morales [b], S. Visacro [c], M.M.F. Saba [d], S.J. Goodman [e], E. Williams [f], M. Peterson [g], N. Pineda [h], M. Arcanjo [i], D. Aranguren [j]

[a] Dept. of Electrical Engineering, Universitat Politècnica de Catalunya (UPC), Terrassa, Spain
[b] Departamento de Ciências Atmosféricas, Universidade de São Paulo, São Paulo, Brazil
[c] LRC-Graduate Program in Electrical Engineering, Federal University of Minas Gerais, Belo Horizonte, Barzil
[d] National Institute for Space Research (INPE), São Paulo, Brazil
[e] Thunderbolt Global Analytics, Owens Cross Roads, AL United States of America
[f] Parsons Laboratory, Massachusetts Institute of Technology, Cambridge, MA, United States of America
[g] ISR – 2 Los Alamos National Laboratory, Los Alamos, NM, United States of America
[h] Servei Meteorologic de Catalunya and UPC, Barcelona, Spain
[i] Dena Desarrollos S.L. and UPC and UPC, Terrassa, Spain
[j] Keraunos SAS, Bogotá, Colombia

ARTICLE INFO

Keywords:
Satellite
Lightning detection GLM
LMA
ASIM
Power systems

ABSTRACT

Information about lightning activity and its parameters is necessary to design and evaluate the lightning protection of an electrical power system. This information can be obtained from ground-based lightning detection networks that provide information on cloud-to-ground lightning strikes with a location accuracy of few hundred meters. Recently, the first satellite-based lightning optical detectors are operating continuously from geostationary orbits. These imagers observe the luminosity escaping from clouds to detect and locate total lightning activity with a spatial accuracy of several kilometers. This allows delineating the initiation and propagation (sometimes over tens to hundreds of kilometers before striking the ground) not observable by the ground-based networks. In this paper, we explore the use of this new technology for lightning protection in power systems. We focus on tall objects such as wind turbines and overhead transmission lines. We show how the optical detections allow identifying lightning flashes that likely produce continuing currents. This provides additional information for the identification of dangerous events and also can be used to estimate the number of upward-flashes from tall objects triggered by a nearby flash. The analysis of a transmission line shows the concentration of faults in the areas of high total lightning flash density. We found regional variations of the optical energy of the flashes along the line.

1. Introduction

The design and evaluation of the performance of a lightning protection system requires the knowledge of the activity and parameters of lightning (e.g. [1–3]. Lightning protection standards benefit from the data provided by lightning location systems (LLS) [4] which principally provide data on cloud-to-ground (CG) strokes. Common lightning location systems are networks of electromagnetic receivers at frequencies from ELF to VHF that resolve the locations of the electromagnetic radiation source by means of techniques such as the time-of-arrival, magnetic direction finding or interferometry [5]. Despite the fact that electromagnetic (RF) detection of lightning is as old as radio, modern operational lightning detection systems only became popular beginning in the 1980′s and are currently available in a large number of countries and some networks even provide global coverage (e.g. [6]). Although such lightning detection systems have significantly improved over the last forty years, the performance of these systems highly depends on the network configuration, its sensitivity and the prevalence of electromagnetic noise sources. Networks covering large areas operating at VLF and/or LF provide mostly detections of CG strokes and some ‘stroke-like’ emissions from in-cloud (IC) lightning processes (e.g. [5]). 2D/3D-mapping of lightning leaders is commonly

* Corresponding author.
E-mail address: joan.montanya@upc.edu (J. Montanyà).

https://doi.org/10.1016/j.epsr.2022.108730
Received 10 February 2022; Received in revised form 31 July 2022; Accepted 11 August 2022
Available online 6 September 2022

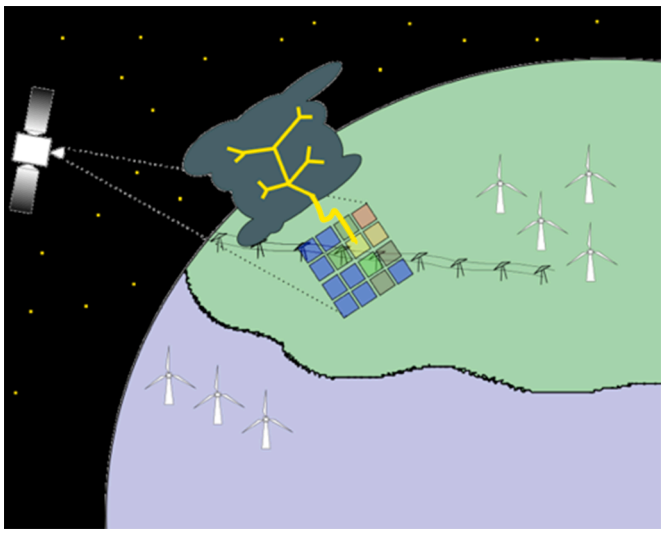

Fig. 1. Sketch of lightning detection from space (proportions are not to scale).

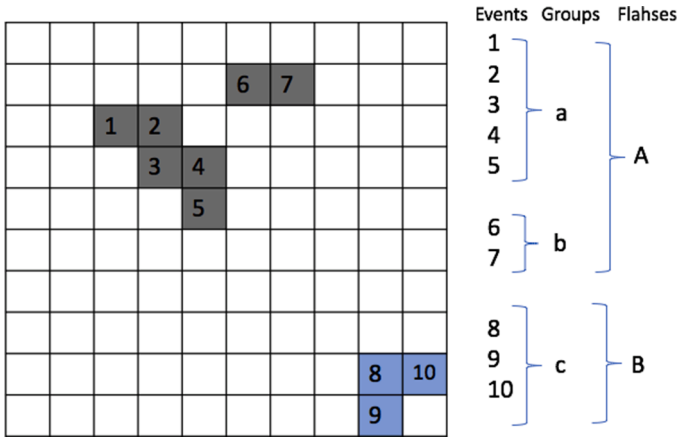

Fig. 2. Events 1 to 10 are detected during a frame. Adjacent events form the groups a, b and c. Two flashes (A and B) are classified because groups a and b are separated in distance by more than 16.5 km from group c.

performed in the VHF band, and is limited to small regions. This is the case of the Lightning Mapping Array (LMA) [7] and VHF interferometry [8].

Following several research efforts prior to the 2010s, detection of lightning from space has now been accomplished for operational purposes. This endeavor started more than 50 years ago with the first optical observations by the OSO 2, OSO 5 and DMSP satellites (see summary in [9]). Later, the Optical Transient Detector (OTD) on the OV-1 satellite provided lightning detection across the globe from 1995 to 2000 from a low-earth orbit with an inclination of 70°. The OTD had a field of view of 1300×1300 km^2 with spatial resolution of 10 km and detection efficiency better than 50% [10]. The successor of the OTD was the Lightning Imaging Sensor (LIS) operated from 1997 to 2015 onboard the TRMM satellite flying in a low-earth orbit with 35° of inclination [11]. The field of view of the LIS was 600×600 km^2 with a nadir pixel resolution of 4 km. Both the OTD and the LIS had a 128×128 pixel CCD with time resolution of 2 ms (500 fps) and observed in a narrow band (1 nm) at 777 nm (atomic oxygen line). After the LIS on the TRMM, a second LIS instrument was mounted on the International Space Station in 2017 [12] and remains in operation today together with the science instrument Modular Multispectral Imaging Array (MMIA) of the Atmosphere-Space Interactions Monitor (ASIM) [13] for high resolution lightning observation. The experience gained from OTD and LIS was leveraged in the development of the Geostationary Lightning Mapper (GLM), and the first of these lightning imagers in a geostationary orbit has been operational the GOES 16 satellite in 2017 [14]. GLM provides continuous observations over the Americas between 54° S and 54° N latitude with a time resolution of 2 ms. The GLM CCD is a 1372×1300 pixel imager that provides 8 km spatial resolution at nadir. Currently, GLM has two instruments, one onboard of the GOES-16 satellite (GOE-S-East at 75.2° W) and one on the GOES-17 satellite (GOES-West at 137.2° W) extending the coverage beyond the American continent to include a large portion of the Atlantic and the Pacific Oceans. In Asia, since 2017, the Lightning Mapping Imager (LMI) on the Feng-Yun-4 (FY-4A) satellite provides lightning detections over a region over China and Australia [15]. The LMI provides images with its 400×300 pixel CCD every 2 ms with a spatial resolution of 7.8 km at nadir. In the coming years, Europe and Africa will be covered by a Lightning Imager (LI) onboard of the Meteosat Third Generation (MTG) [16]. The expected pixel resolution of the MTG-LI will be 4.5 km at the sub-satellite point with a frame rate of 1 kHz (1 ms). Both LMI and LI also use the 777.4 nm line for lightning detection.

The application of satellite lightning data collected by these satellites to the lightning protection problem is not new. Climatology products based on OTD/LIS observations have been recommended to estimate the ground flash density (Ng) in otherwise data-sparse regions of the Earth [2,3]. These data have been produced by the accumulation of a large number of short periods of observation at a given location due to the low-earth orbit of the available satellites (e.g. TRMM LIS VHR Climatology Data Sets available from the NASA Global Hydrology Resource Center -GHRC0). The collection of continuous lightning measurements from geostationary orbit marks a new era of lightning detection where lightning is monitored continuously over large swaths of the Earth.

In this paper we propose the use of space-based lightning detections in the context of electrical power systems beyond the climatological data that has been used previously. We first introduce the characteristics of the satellite-based lightning data. We present a comprehensive example of a flash detected simultaneously from space and ground to highlight the differences between the detections provided by space and ground-based systems. Next, the application of satellite lightning data to power systems is organized in four parts. The first part deals with the detection of flashes with continuing currents, the second with lightning strikes to tall objects, the third part is about lightning strikes to an overhead transmission line and the last, on the application to lightning warning.

2. Satellite-based lightning detection

2.1. Data products

Satellite-based lightning detections generate similar data products for the different instruments. We select GLM to present the data format and the examples. GLM data is organized into different processing Levels. Level 0 data is the lowest data level that comprises the ‘raw’ lightning data from the optical sensor. Level 1 data are generated from the Level 0 data by performing radiometric and geometric corrections. Finally, Level 2 data construct the final data products for end users. Level 0 and Level 1 data only include the most fundamental element of GLM detection: the ‘event’. Events consist of large numbers of non-lightning triggers, plus events due to legitimately to lightning. Data processing aims to identify lightning events and reject non-lightning related events. Hereinafter we will refer as events to those produced by lightning. The events correspond to single-pixel detections of lightning during a single 2-ms integration frame. Each of the numbered boxes inFig. 2 corresponds to unique events. The Level-2 data clusters the events into complex features that describe different aspects of lightning activity. Events in the same integration frame are clustered first into “groups” corresponding to contiguous regions that are simultaneously illuminated (colored region in Fig. 2) that approximate distinct lightning

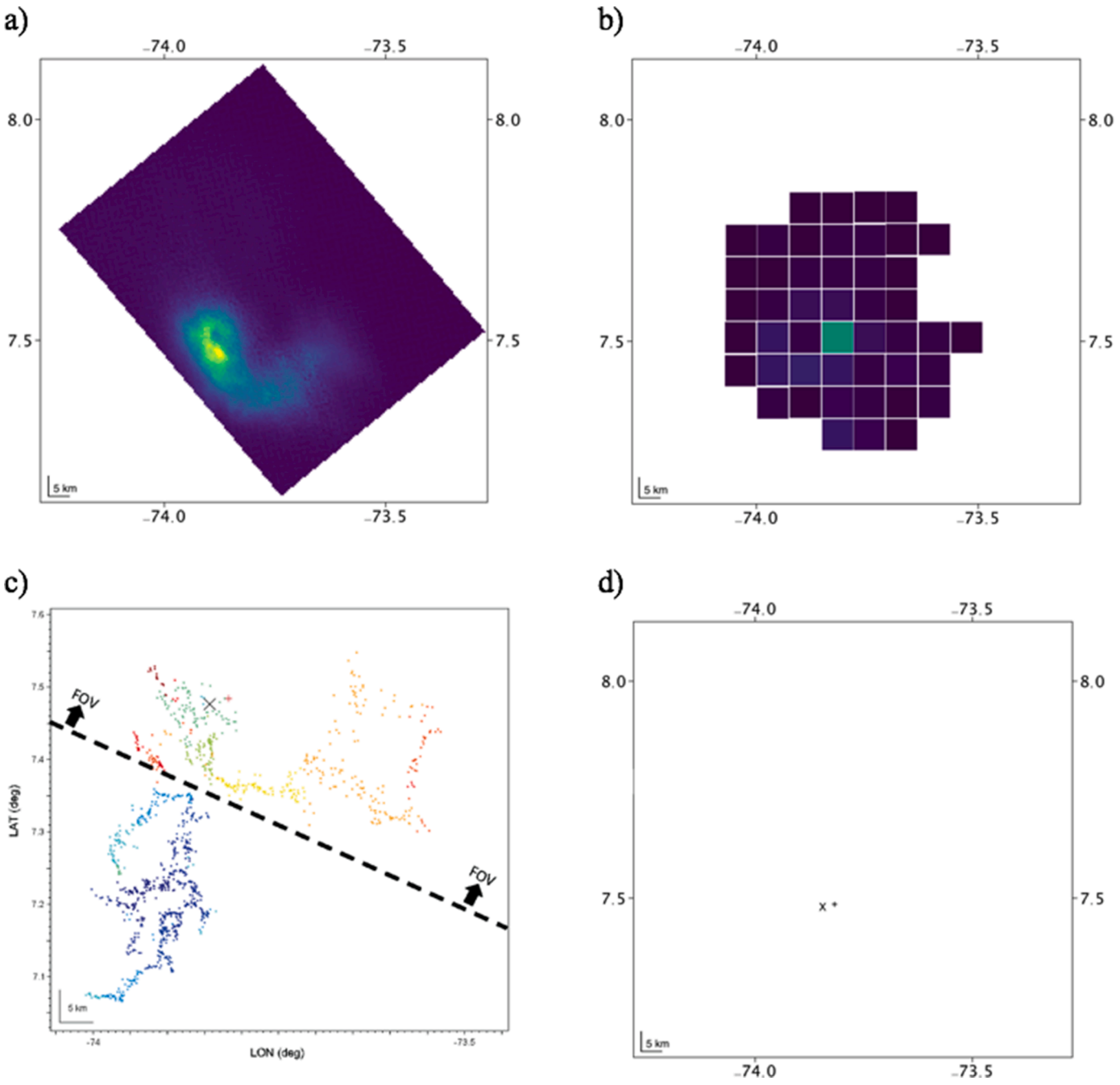

Fig. 3. Case of the flash on 20,181,122 at 08:57:21.4 UT in Colombia. a) Composition of 777.4 nm camera of ASIM-MMIA; b) GLM events; c) Lightning Mapping Array, the dashed line showing the FOV indicates the portion of the flash imaged by ASIM-MMIA in (a) and selected from GLM in (b); d) VLF/LF cloud-to-ground detections by a LLS. Data are adapted from [24].

pulses. Groups are then clustered into "flashes" based on their temporal and geospatial proximity to one another (e.g. sequential occurrence of groups in less than 330 ms and in space by no more than 16.5 km) [14]. The locations of groups and flashes are determined by computing their radiance-weighted centroid positions. Finally, gridded derived products are generated from the Level 2 data that aim to satisfy most of the end user needs (e.g. [17]). These gridded products include: Flash Extent Density, Minimum Flash Area, Total Optical Energy (radiance), Event Density, etc.

2.2. Performance metrics

Lightning detection from space has the advantage of covering a large area with high detection efficiency (DE). However, optical lightning detectors from space are not perfect; neither ground-based RF nor space-based optical instruments are 100% detection efficiency-effective. The selected spectral band of 777.4 nm with narrow bandwidth (one or a few nm) allows for observations in both day (against a bright sunlit cloud top) and night. The detection technique is commonly based on the comparison of an actual image frame with a background image. There are several factors that reduce the detection efficiency. One factor is related to the nature of thunderstorms and lightning. Some lightning flashes occur at low levels of the clouds where attenuation causes the signal to fall below instrument threshold. The cloud ice water path and optical depth may also result in signal attenuation.

Another important aspect is the False Alarm Rate (FAR) that

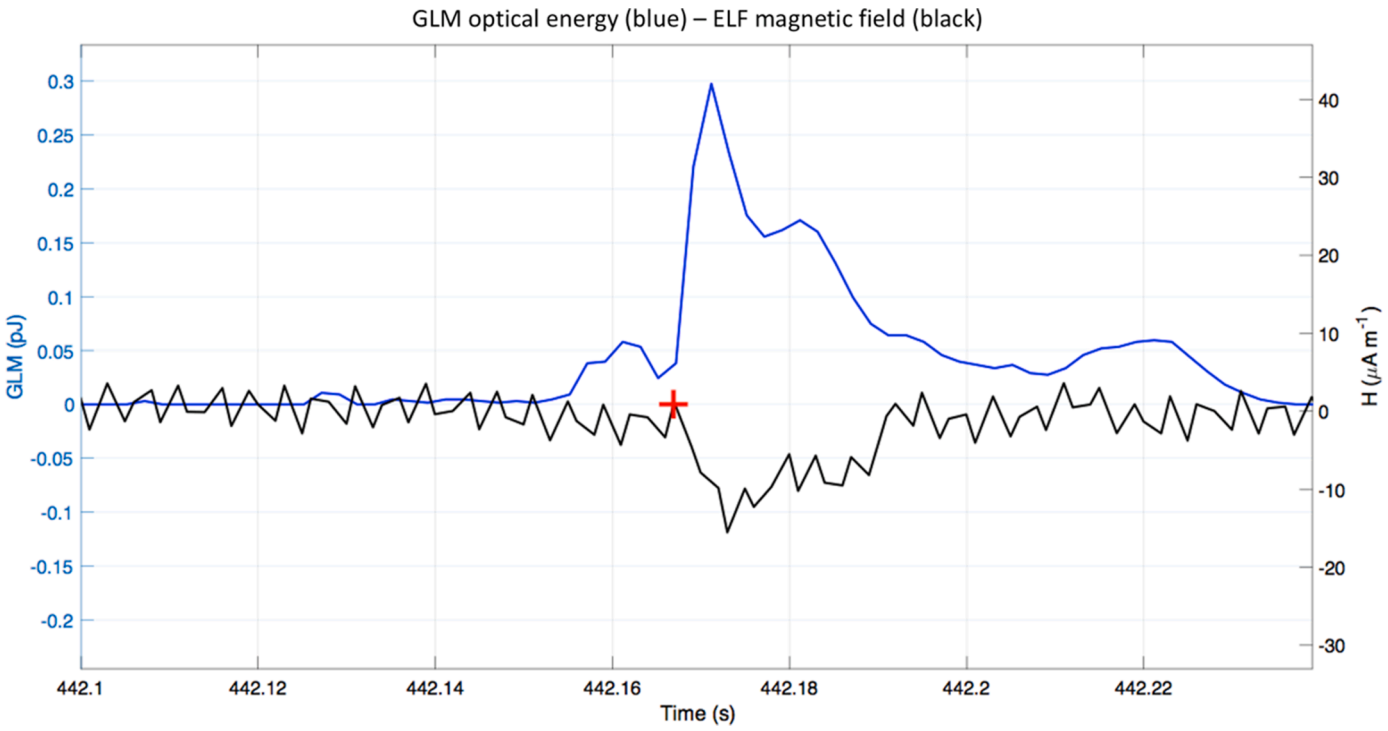

Fig. 4. In blue, GLM optical energy computed by integrating the energies of all the events for each individual frame. In black, ELF magnetic field measured from the UPC Cape Verde's Schumann resonance station. The red plus corresponds to the LLS detection of a positive CG. Data are adapted from [24].

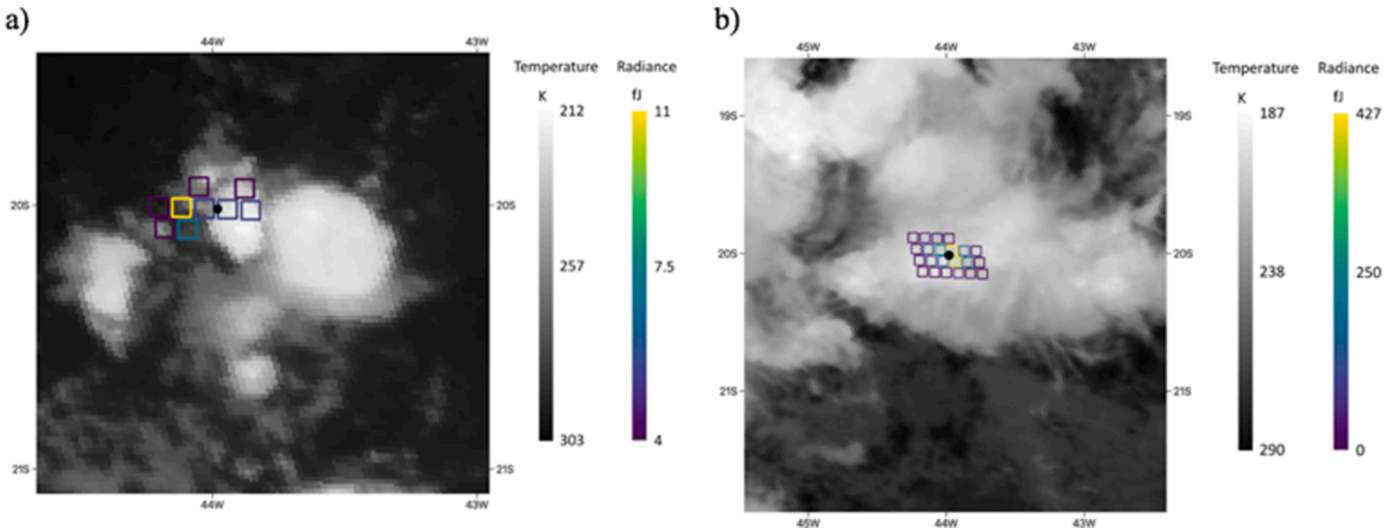

Fig. 5. Two examples of GLM detection of flashes at the Morro do Cachimbo instrumented tower in Belo Horizonte (Brazil) overlayed with GOES-16 ABI infrared satellite image; a) Flash on 20,190,120; b) Flash on 20,180,224. Pixels are colored by the maximum radiance (energy). Note that the pixels are simplified by squares.

measures how well the instrument is rejecting non-lightning events. In addition to lightning, a great deal of sources can trigger single pixels producing false lightning events. This is the case of noise sources such as artifacts produced by solar light contamination, sunglint or instrument artifacts (e.g. [18] and [19]). In some cases, even post processing data cannot eliminate these false events. Ongoing efforts have been recently summarized in [20].

Finally, the Location Accuracy (LA) is another important aspect to consider in space-based instruments. Since lightning locations are obtained from images, these have a resolution according to the number of pixels of the sensor, optical assembly and the distance of the satellite to Earth. Moreover, the height of the radiant emitter also affects the geolocation of lightning flashes. Cloud-top-height needs to be known or assumed to minimize parallax errors. GLM location accuracy has been verified to a half pixel (~5 km) near nadir to a larger error towards the limb [21,22]. As a practical example, evaluation of the ISS-LIS by the Ebro-Lightning Mapping Array can be found in [23].

3. Comparison of ground-based and satellite-based lightning detections

Lightning is detected from space due to the illumination of the surrounding clouds. This detection method is substantially different than the radio electromagnetic methods used by lightning detection systems that directly detect lightning discharges. This unique aspect of the optical space-based lightning detection can be used to provide new

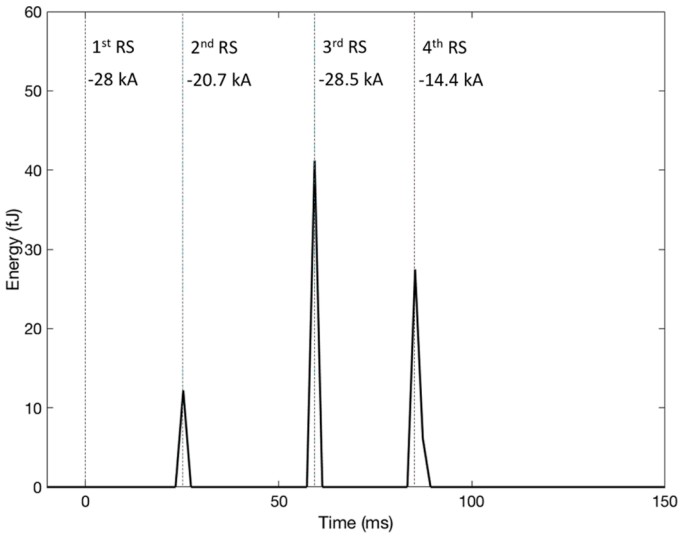

Fig. 6. GLM frame-integrated optical energy and measured return stroke peak currents of the flash on 20,190,120 (20:15:27 UT) at the Morro do Cachimbo tower.

information for operational purposes. To illustrate how the same flash is detected from space-based and ground-based systems, Fig. 3 presents the detections of a single lightning flash. This lightning flash was detected from space by ASIM-MMIA on the ISS and by GLM (for more information see [24]). From the ground, the flash was in the range of the VHF Colombia-Lightning Mapping Array (LMA) and by a VLF/LF lightning detection system (Linet-Keraunos [25]).

4. Use of satellite-based data for lightning protection

As seen in the example in Fig. 3, satellite optical imagers observe total lightning (IC and CG lightning) but cannot (currently) uniquely identify flash type (IC or CG strike) nor provide the locations of CG strikes with precision location accuracy. On the ground, each pixel has already a size of several kilometers (e.g. 8 × 8 km), so it is not possible to achieve a similar accuracy on the order of a few hundred of meters such as in ground-based lightning detection systems. Additionally, the fact that lightning is observed from the top and sides of the cloud means that it is not currently possible to accurately identify the presence of a CG stroke without coincident measurements from a ground-based lightning location system. In contrast with ground-based lightning detection systems, with the exception of small VHF networks such as the LMA, satellite data can provide detections of total lightning including the in-cloud development of individual flashes. For each lightning flash, the extension and duration can be determined as well as a set of properties derived from the optical emissions.

In this section, we present examples of the application of GLM data interesting for electric power systems.

4.1. Identification of continuing currents

The presence of continuing currents in lightning strokes pose one of the major threats to electric power systems due to their high energy content. In particular, continuing currents can cause major damage to wind turbine blades (e.g. [26,27]). In the wind energy industry, the occurrence of severe damage to wind turbine blades by lightning strokes with low peak currents but with continuing current is widely recognized. Unfortunately, continuing currents do not produce electromagnetic radiation often detected by VLF/LF lightning location networks. So, the presence of continuing currents is missed by lightning location systems. Probably the most promising contribution of space-based optical detectors is the capability to identify long continuing currents which are responsible for most serious lightning damage associated with thermal effects and that is present in approximately 30% of negative CG and in 75% of positive CG [28,29].

Using the LIS, in [30], flashes with continuing currents were identified with the signature of at least five sequential contiguous groups. This assumption was verified against one electric field measurement, so it cannot be concluded that the identified LIS flashes with contiguous optical signals are actually continuing currents events involving CG strokes or some other long-duration in-cloud activity. Recently, in the simultaneous observation by ASIM, GLM and LMA presented in [24], continuing current was identified from GLM data by continuously integrated optical energy after a positive CG stroke. In that case, data from an ELF station confirmed the presence of continuing current in the event. Fig. 6 displays the GLM radiance and the ELF magnetic field waveform for the case presented in [24].

Efforts are underway to combine the high spatial accuracy of ground-based RF detection and location with the continuing current detection provided by the operational space-based optical lightning imagers such as GLM (see [31]). In the next section, +CG flashes with continuing currents will be examined in the context of upward-triggering lightning flashes.

4.2. Lightning strikes to tall objects

Lightning to tall objects has been one of the concerns of the CIGRE WG C4.410 [32], WG C4.409 [27] and WG C4.36. Firstly, we investigate flashes occurring at the instrumented tower at Morro do Cachimbo in Belo Horizonte (Brazil). This 60 m instrumented tower provides current measurements of direct lightning strokes. In Fig. 5 we present two examples of GLM detections of flashes striking the Morro do Cachimbo tower.

The two examples in Fig. 5 show the maximum optical energy among all the events at each pixel. The two flashes are properly detected and the maximum energy is also detected at the tower location or nearby. To find any relation between the CG stroke occurrence and the optical radiances reported by the GLM, in Fig. 6 we present the time-integrated energy (integrated optical energy of all the events during the same frame) versus the peak currents measured at the tower. In the example, the first return stroke was not detected by the GLM although the peak current was higher than other two of the three subsequent strokes. Each of the subsequent strokes had an associated luminosity pulse in the GLM observations. The missing detection of the first RS might be attributed to the fact that some CG flashes start at low cloud altitudes that can significantly attenuate the luminosity from the lightning channels. During the rest of the flash, lightning leaders can extend and reach higher altitudes, thereby being more detectable. For more details about detections of IC and CG by GLM and LIS read the results and the discussion in [33].

The fact that in the flash in Fig. 6 there are no previous GLM detections suggests that this corresponds to flash initiated in the lower parts of the cloud and a downward negative leader striking the tower as is frequently observed at Morro do Cachimbo (84% reported by [34]). But a second mode of lightning occurs at tall towers [34]. This case corresponds to a lightning-triggered upward lightning in which a nearby flash triggers upward leaders from the tower ([34–38] among many other references). Typically, upward positive leaders are initiated from towers as a response to the charge removal of positive strokes and their following continuing currents sustained by in-cloud negative leader development [39].

In order to explore the characteristics of the upward-triggering lightning flashes, we have analyzed several high-speed video recordings of upward flashes at Pico do Jaraguá towers (São Paulo, Brazil) [36,40]. Fig. 7 presents two upward flashes triggered by nearby positive CG flashes. Figs. 7a and c depict the GLM events location for each +CG flash. The color of the squares corresponds to the maximum energy of the events in the pixel. The location of the +CG stroke and the towers is

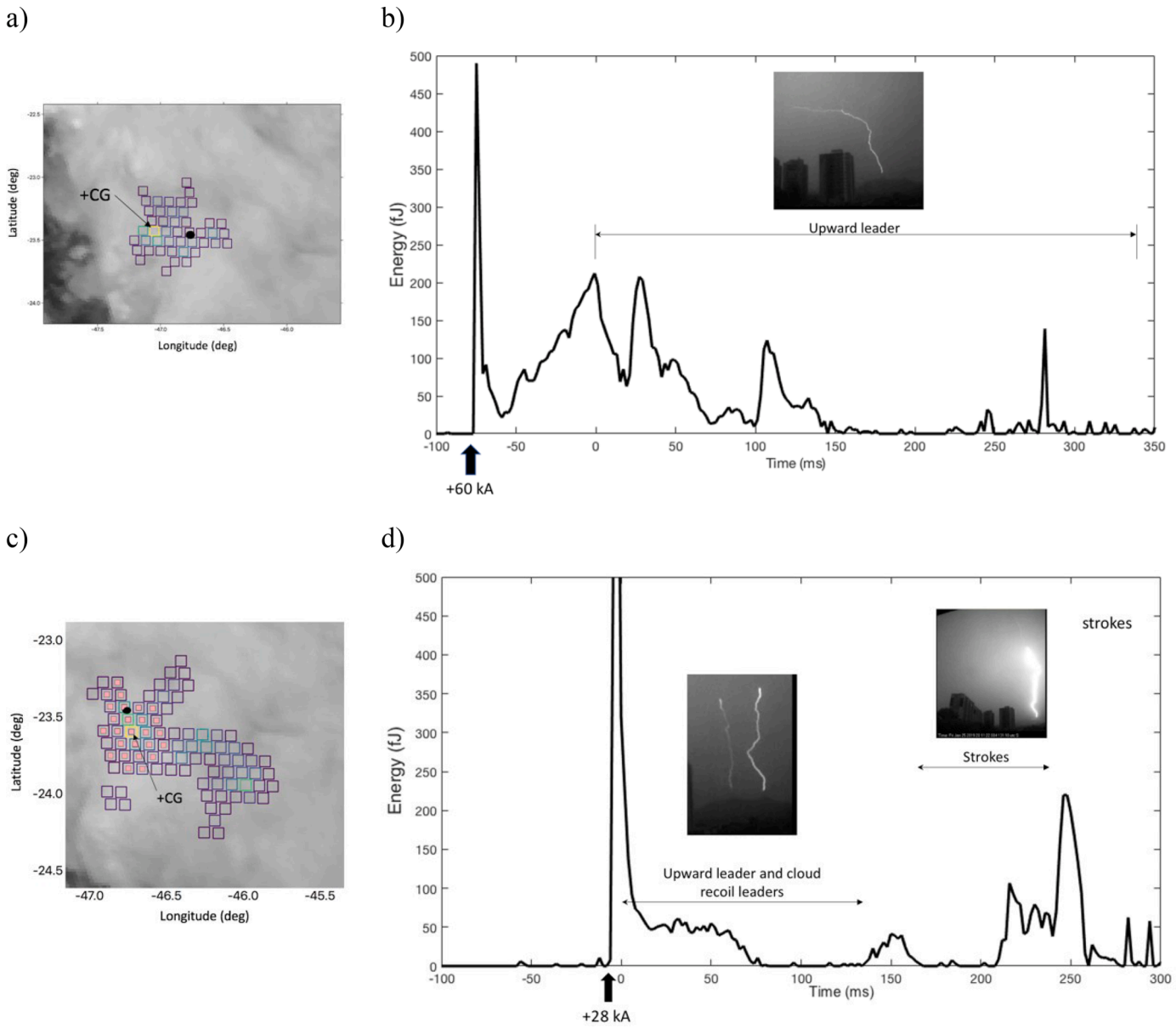

Fig. 7. Two upward-triggering lightning flashes at Pico do Jaragúa towers (São Paulo, Brazil). a) GLM detections of the first flash. The location of the GLM pixel corresponding to the location of the +CG stroke is indicated. The circle marker indicates the location of the towers. b) GLM frame-integrated optical energy for the first flash. c) and d) correspond to the second flash.

indicated in each figure. In the first flash (Fig. 7a) the distance of the +CG stroke to the tower is three GLM pixels (~30 km), whereas in the second flash the distance is two GLM pixels (~20 km). Fig. 7b shows that the upward leader at the tower initiated 75 ms after a +CG stroke of 60 kA followed by continuing current according to the integrated GLM optical energy. In this delayed case, the initiation was probably due to the cloud charge removal close to the location of the tower by negative leader activity involved with the supply of continuing currents [36,40] or the influence of a negative leader itself [35,40]. In the second flash (Fig. 7d), the upward leaders from the towers started shortly after the stroke. In that case the location of the +CG was closer than in the other flash. That might explain the short delay between the stroke and the upward leaders. The first flash did not produce strokes along the upward leader to ground, whereas the second flash, after 160 ms several strokes reaching the ground were observed in the video.

As in Fig. 4, Figs. 7b and d show a strong energy peak related to the return stroke followed by a continuous luminosity period related with continuing current. In one case the luminosity remained for more than 200 ms after the stroke.

The triggering scenario provided by the detection of a +CG stroke followed by continuous GLM luminosity (Fig. 7) can be used to estimate the frequency of occurrence of potential upward-triggering lightning flashes. This can be useful to estimate the exposure of tall objects such as wind turbines. To illustrate an example, we have selected the CN Tower in Toronto (Canada), which is well-known for its lightning triggering (e.g. [41]). For all the flashes detected by GLM during 2019–2021, we have analyzed the presence of flashes that potentially presented continuing currents with a simple method. For each flash, the frame-integrated optical energy is computed (e.g. Fig. 7b), and the peaks above a certain threshold are identified (200 fJ in this case). We assume that a flash has continuing current if the luminosity (optical energy) does not return to zero before 10 consecutive frames (20 ms) after a peak. The result of the distribution of these flashes is plotted in the map of Fig. 8. In the plot, the pixels are colored with the average number of flashes that potentially produced continuing currents illuminating that pixel. The map shows a region in the east of St. Catharines (Canada) where the

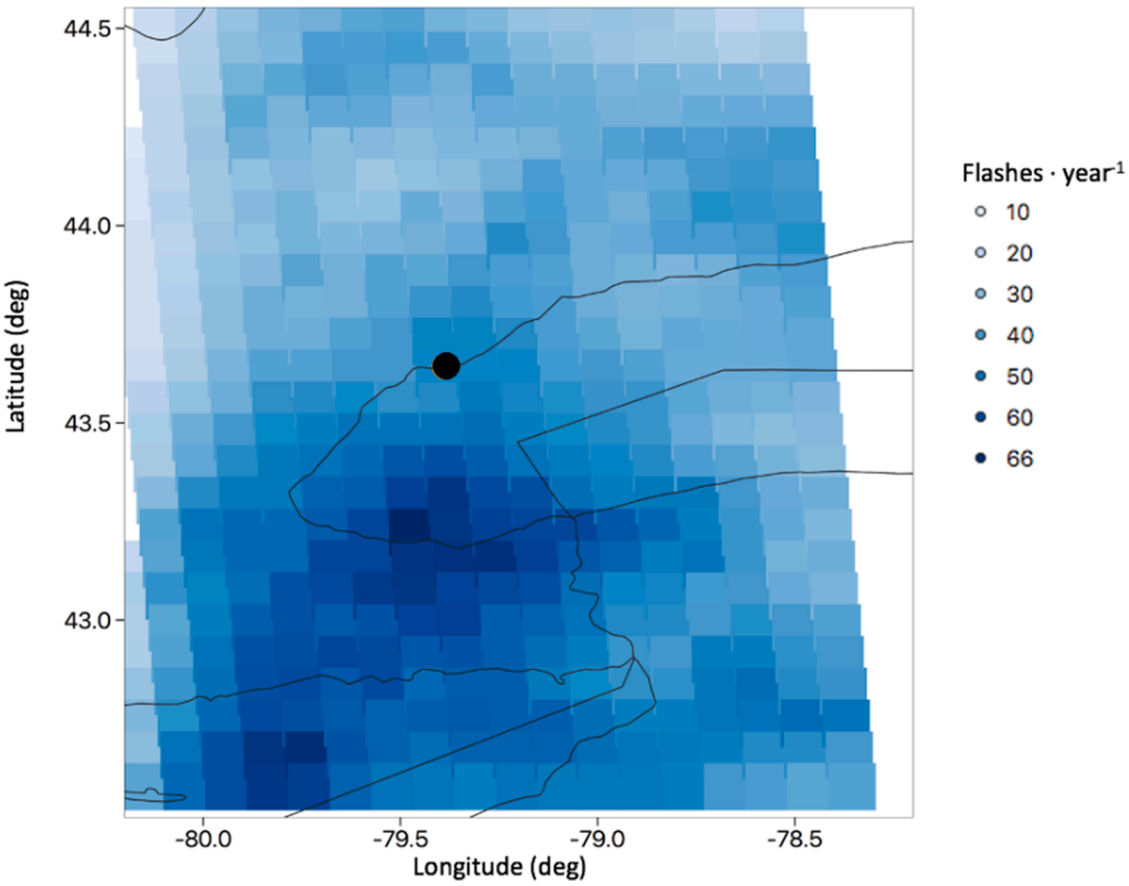

Fig. 8. Average anual number of flashes that potentially produced continuing currents for each GLM pixel in the area of Toronto. The round marker indicates the location of the CN Tower.

flashes with continuing currents are more frequent. So, we can see that the CN Tower is close to a region with more frequent lightning that might involve continuing currents. As we have seen from the cases in Fig. 7, a flash with a CG stroke located several tens of km from the tower can still influence the initiation of upward leaders. This is because the in-cloud leaders of a flash (mainly those associated to the continuing current that follows a +CG stroke) can typically extend several tens of kilometers [40, 39]. According to the map, the conditions for upward lightning at the CN Tower due to a nearby flash can be present more than 40 times per year.

In Europe, lightning at towers is often upward-initiated from the tower (e.g. [26,42]). Unfortunately, there is no published information about the self-initiated flashes at the CN Tower and our analysis using GLM did not show evidences. We expect that self-initiated upward lightning from tall objects would be more difficult to observe from satellite platforms since in many cases upward leaders remain lower in the cloud. But the common occurrence of upward lightning in shallow stratiform regions [26,42] might allow some light to escape from the cloud to be detected aloft. Space-based observations of self-initiated upward lightning need further investigation.

4.3. Total lightning exposure of electric power systems and other targets

One of the advantages of detecting total lightning from space with a wide coverage is to determine the exposure to lightning of large power systems and other particular targets of interest. Here we will show an example of the lightning activity on a 500 kV overhead transmission power line in Colombia, South America. The total length of this line is 214 km, with 425 towers at altitudes from 500 to 2800 MSL. The first 100 km are characterized by complex orography conditions with the highest terrain altitudes while the second power line section presents a quite constant altitude around 1100 MSL. Such transmission lines, (500 kV and higher) are known to have robust isolation capable of withstanding almost all of lightning strikes. However, power failures in this specific case are caused by back-flashovers due to direct lightning strikes on the tower or the grounded wire with critical lightning peak currents varying in each tower from 42 to 96 kA, where the lowest critical peak currents correspond to towers on the first 120 km. In addition, shielding-failure flashovers (phase wire lightning strikes) are also more recurrent in the first 100 km section [43]. Fig. 9 displays the total lightning flash density for the period of 2019–2021 in the region of the transmission line. Each grid cell corresponds to the area observed by the corresponding GLM pixels. Along the line, the locations of the faults reported for these two years are indicated as red squares.

The total flash density along the transmission line is depicted in Fig. 10. Flash density is calculated as the annual average number of flashes that had at least one event in the pixel containing a segment of a power line divided by the area of the field of view of the pixel. The highest lightning density is found along the first 70 km with a maximum of 450 flashes km^{-2} $year^{-1}$ at ~20 km. The start of the line is located very close to one of the lightning hot-spots in Colombia [25]. Almost half of the total faults are concentrated in the first 65 km, corresponding to the area with the most complex orography and lowest critical peak currents for failure. The flash density decreases to a minimum of 125 km^{-2} $year^{-1}$ at 100 km. Some faults occur in the region of low flash density (80–160 km) but these are more widely distributed. At 175 km, the flash density rises again reaching a peak of 220 flashes km^{-2} $year^{-1}$. This peak is accompanied with a concentration of faults located between180 and 210 km. Comparing the total lightning flash density with the CG lightning flash density in Colombia [25], we found an order of

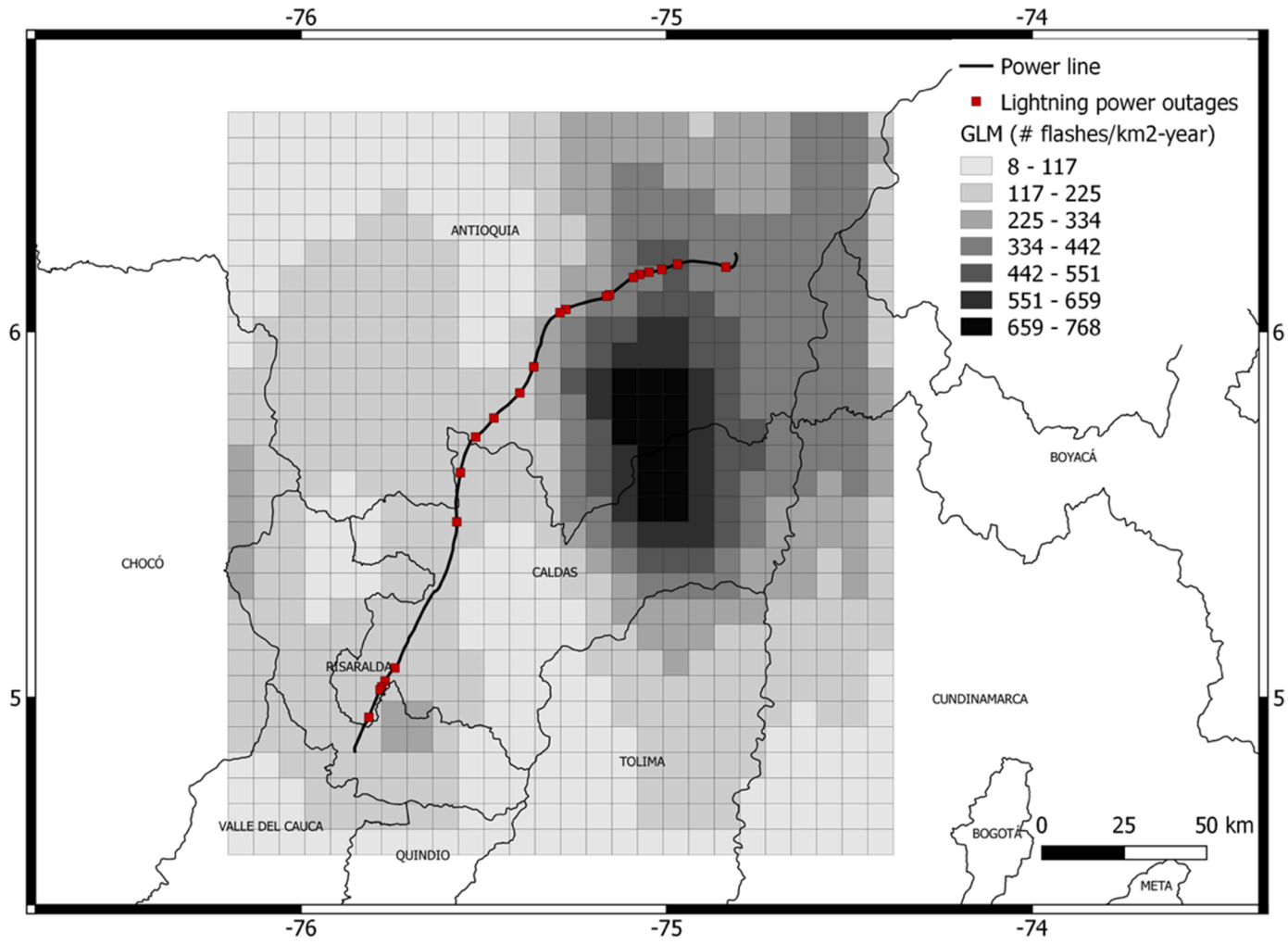

Fig. 9. Total lightning flash density in the region of a 500 kV transmission line (solid line) for the period 2019–2021 from GLM data. The location of the line faults for a period of two years are indicated with red squares.

magnitude difference between the total lightning density from GLM (Fig. 9) and the CG flash density.

In addition, we have computed the average total optical energy of the flashes in the grids along the transmission line (Fig. 10). The average total energy corresponds to integrating the energies of all the events in the pixel (grid cell) for each flash. We found that this optical energy is not uniform along the line. The flashes along the first 75 km of the line present higher optical energies than the rest. Although this preliminary finding is not yet confirmed, this might be indicative of the presence of more energetic CG flashes (see [24]).

Here we have provided a simple example. In Fig. 9, we just considered the data of the corresponding pixels intersected by the power line. However, alternative methods can be proposed, including the weighting of the data of the adjacent pixels according to the position of the power line within the pixel (e.g. cases where the power line is located close to the boundary or to a corner of a pixel). Also, the events can be selected according to the maximum optical energy (e.g. only including the event with the maximum energy or those over some prescribed threshold). In addition to the lightning activity, space-based lightning imagers can provide new information that can be used to evaluate the performance of a power line. While not being exhaustive, we propose:

i) Documentation of lightning activity of flashes potentially involving continuing currents with the methodology presented in the previous section. Properties such as duration and total optical energy of the continuing currents can be considered.
ii) Identification of long flashes that 'illuminate' large areas along the power line including those individual flashes that can produce many tens of strikes to ground (e.g. [44]).
iii) Computation of the duration of the flashes along the power line.

So, satellite data can be useful to identify those types of flashes, not strictly involving CG strokes, in which a large amount of electric charge is neutralized or transferred to ground implying intense electrostatic field changes along large extents of the power line. In addition, as it has been mentioned, further investigations are needed to relate the intense events with CG strokes.

4.4. *Lightning warning*

Data from operational space-based lightning imagers provide a powerful tool to produce lightning warnings in electrical power systems. The methods can be just the ones provided in the standard IEC 62,793 [45] with the following advantages:

- Continuous coverage of very large transmission lines is possible.
- Total lightning instead of CG alone, or a small portion of IC flashes thereby reducing the failure to warn. Also, a lightning flash is not presented as a discrete location, the extension (area) of the flash can be included in the warning method.

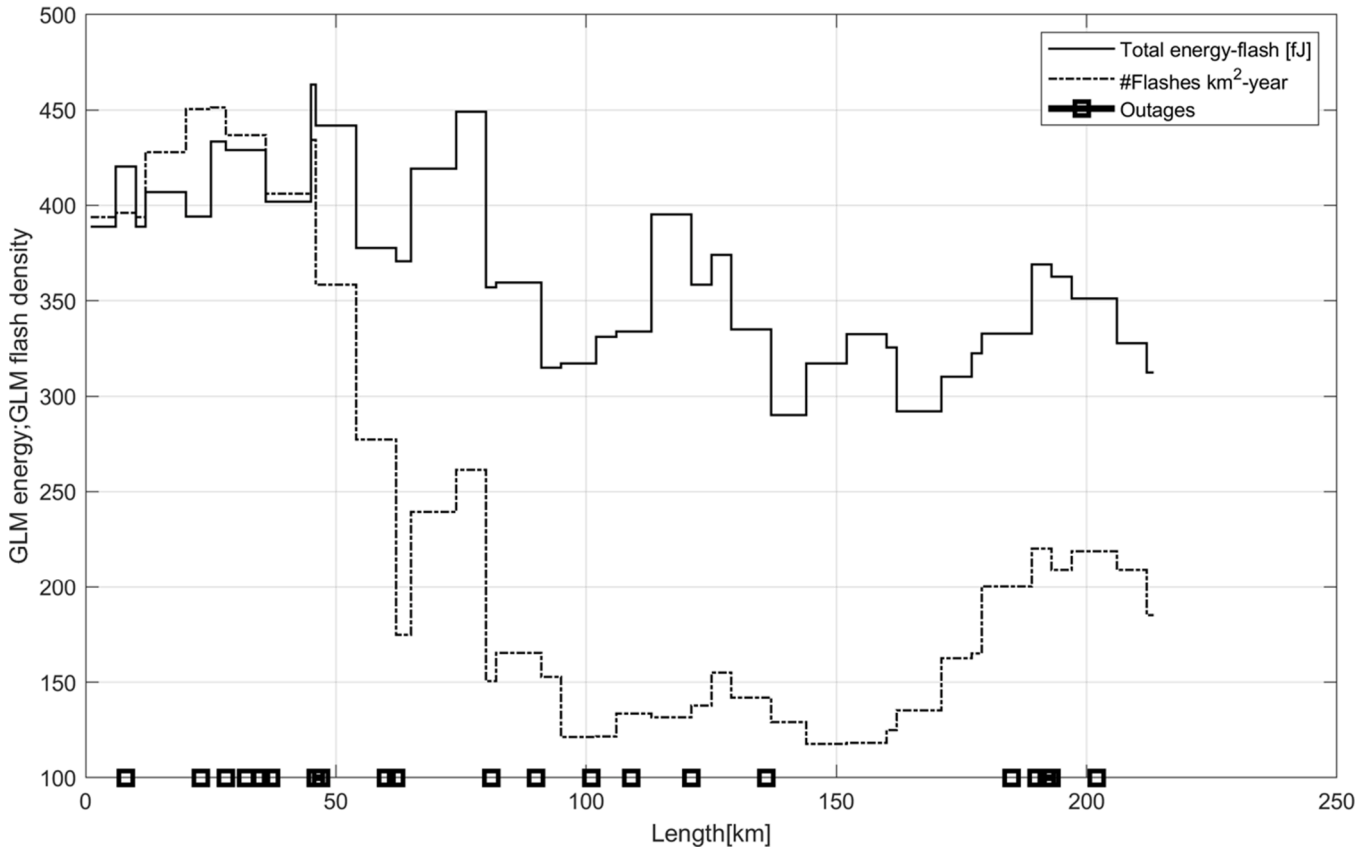

Fig. 10. Lightning activity on the 500 kV transmission line during April 2019. The dash-dotted line corresponds to the annual average number of GLM flashes that had at least one event in the pixel containing a segment of the power line divided by area of the field of view of the pixel.

- Identification of "megaflashes". Some high-resolution ground-based VHF systems are limited to small areas, so flashes covering large distances, e.g. more than a few hundred km, cannot be totally traced.
- Reliability in terms that are not dependent on the available number of sensors, the geometry of the network and the noise levels such as in lightning location networks.

The listed features can be useful in lightning warning in electrical power systems offering additional information to the ground-based lightning location networks allowing to allow better characterization and identification of line fault risk. Summing up:

- Lightning detection in regions not covered or poorly covered by lightning location systems.
- More realistic quantification of the total lightning activity over large areas.
- More realistic characterization in size and duration of lightning flashes in large areas.
- Possibility to identify continuing currents.

5. Conclusions

A new era in the detection of lightning has arrived thanks to the space-based operational lightning imagers. These systems offer a new perspective on lightning detection that can be used in electric power systems. The main features of space-based lightning imagers can be summarized as follows:

- Total lightning information is provided: satellite optical imagers observe the illuminated cloud tops and edges due to lightning.
- Very large coverage (e.g. all of the Americas).
- The spatial resolution is related to the area at the cloud top level covered by a pixel of the optical imager (e.g. 10×10 km).
- Time resolution is typically 2 ms or 1 ms.
- Size and duration of the flashes can be resolved.
- Lightning processes involving continuing currents can be identified.

Some applications of this data have been presented in the paper. We have shown examples of GLM detections of flashes involving continuing currents. The identification of continuing currents allows extending the lightning risk assessment to the contribution of energetic flashes. This can be important for selecting surge arresters' charge and energy capabilities. The occurrence of flashes with continuing currents can present a threat to wind turbines due to the high energy content of the currents. In addition, the frequency of flashes with continuing currents at locations of wind farms, wind turbines or tall objects can help estimate the number of upward-triggering lightning flashes. More research is needed to determine if self-initiated upward flashes can be identified from space-based instruments. These flashes occur typically in winter conditions, and the observed upward leaders remain lower in the cloud.

In the case of overhead transmission lines, we have presented the total flash density along a line for a three-year period. The total flash density computed with GLM data is an order of magnitude higher than the cloud-to-ground flash density found in the literature for the same area. For engineering applications, it is essential to distinguish between mean annual lightning flash density as provided here with the mean annual lightning flash rate density provided by low-earth orbit instruments (e.g. LIS). For instance, in the estimation of the CG flash density. Regarding the locations of the faults, we found that they are more frequent in the regions with higher total flash density. In particular, the number of faults per kilometer is higher in areas with higher flash density. Besides the variation of the flash density along the line, we

found that the optical energy of the flashes also changes regionally.

CRediT authorship contribution statement

J. Montanyà: Conceptualization, Formal analysis, Writing – original draft. **J.A. López:** Visualization, Methodology. **O. van der Velde:** Methodology. **G. Solà:** Methodology. **D. Romero:** Writing – review & editing. **C. Morales:** Writing – review & editing, Methodology. **S. Visacro:** Data curation. **M.M.F. Saba:** Data curation. **S.J. Goodman:** Writing – review & editing. **E. Williams:** Writing – review & editing. **M. Peterson:** Writing – review & editing. **N. Pineda:** Writing – review & editing. **M. Arcanjo:** Writing – review & editing. **D. Aranguren:** Data curation.

Declaration of Competing Interest

The authors declare that they have no known competing financial interests or personal relationships that could have appeared to influence the work reported in this paper.

Data availability

Data will be made available on request.

Acknowledgements

This work was supported by research grants ESP2017-86263-C4-2-R funded by MCIN/AEI/ 10.13039/501100011033 and by "ERDF A way of making Europe", by the "European Union"; and Grants PID2019-109269RB-C42 and ENE2017-91636-EXP funded by MCIN/AEI/ 10.13039/501100011033. S. Goodman was in part supported by NASA Grant 80NSSC18K1689. M. M. F. Saba was in part supported by research grants 2012/15375–7 and 2013/05784–0, from São Paulo Research Foundation (FAPESP). S. Visacro was supported by a research grant (307381/2019–6) of the Brazilian National Council of Technological and Scientific Development (CNPq). The GLM data are available from the NOAA National Centers for Environmental Information (NCEI) and Cloud Service Providers (e.g., Amazon Web Services, AWS). The LIS data are available from the NASA GHRC Distributed Active Archive Center (DAAC) (https:// https://ghrc.nsstc.nasa.gov/home/access-data. The power system information for the 500 kV transmission line is provided by ISA-INTERCOLOMBIA and is supported by L. Porras.

References

[1] IEC 62305-2:2012: Protection against lightning. Part 2: risk management.
[2] IEC 61400-24:2019. Wind energy generation systems -Part 24: lightning protection.
[3] IEEE Std 1410:2010. IEEE guide for improving the lightning performance of electric power overhead distribution lines.
[4] Diendorfer, G., W. Schulz, C. Cummins, V.A. Rakov, M. Bernardi, F. De la Rosa, B. Hermoso, A.M. Hussein, T. Kawamura, F. Rachidi, and H. Torres, 'Cloud-to- ground lightning parameters derived from lightning location systems – the effects of system performance'," in Electra, 2009, no. 243, Technical Brochure 376 WG C4.404.
[5] A. Nag, M.J. Murphy, W. Schulz, K.L. Cummins, Lightning locating systems: insights on characteristics and validation techniques, Earth and Space Sci. 2 (2015) 65–93, https://doi.org/10.1002/2014EA000051.
[6] K.L. Cummins, M.J. Murphy, An overview of lightning locating systems: history, techniques, and data uses, with an in-depth look at the U.S. NLDN, IEEE Trans. Electromagnetic Compatibility 51 (3) (2009). VOLNO.
[7] W. Rison, R. Thomas, P. Krehbiel, T. Hamlin, J Harlin, A GPS-based three dimensional lightning mapping system: initial observations in central New Mexico, Geophys. Res. Lett. (1999), https://doi.org/10.1029/1999GL010856.
[8] J. Montanyà, S. Soula, N. Pineda, A study of the total lightning activity in two hailstorms, J. Geophys. Res. 112 (2007) D13118, https://doi.org/10.1029/2006JD007203.
[9] H.J. Christian, R.J. Blakeslee, S.J. Goodman, The detection of lightning from geostationary orbit, J. Geophys. Res. 94 (1989) 13329–13337.
[10] D.J. Boccippio, H.J. Christian, Optical detection of lightning from space, NASA Tech. Report (1998). Available in, https://ntrs.nasa.gov/api/citations/19990008509/downloads/19990008509.pdf.
[11] Christian, H.J., and Coauthors, 1999: The lightning imaging sensor. 11th International Conference on Atmospheric Electricity, H. J. Christian, Ed., NASA Conf. Publ. NASA/CP-1999-209261, 746–749.
[12] R.J. Blakeslee, T.J. Lang, W.J. Koshak, D. Buechler, P. Gatlin, D.M. Mach, G. T. Stano, K.S. Virts, T.D. Walker, D.J. Cecil, W. Ellett, S.J. Goodman, S. Harrison, D. L. Hawkins, M. Heumesser, H. Lin, M. Maskey, C.J. Schultz, M. Stewart, M. Bateman, O. Chanrion, H. Christian, Three years of the lightning imaging sensor onboard the international space station: expanded global coverage and enhanced applications, J. Geophys. Res. Atmos. 125 (2020), https://doi.org/10.1029/2020JD032918 e2020JD032918.
[13] O. Chanrion, T. Neubert, I. Lundgaard Rasmussen, et al., The modular multispectral imaging array (MMIA) of the ASIM payload on the international space station, Space Sci. Rev. 215 (2019) 28, https://doi.org/10.1007/s11214-019-0593-y.
[14] Steven J. Goodman, Richard J. Blakeslee, William J. Koshak, Douglas Mach, Jeffrey Bailey, Dennis Buechler, Larry Carey, Chris Schultz, Monte Bateman, Eugene McCaul Jr., Geoffrey Stano, The GOES-R geostationary lightning mapper (GLM), Atmos. Res. (2013) 34–49, 125–126.
[15] J. Yang, Z. Zhang, C. Wei, F. Lu, Q. Guo, Introducing the new generation of Chinese geostationary weather satellites, Fengyun-4, Bull. Am. Meteorological Soc. 98 (8) (2017) 1637–1658, https://doi.org/10.1175/BAMS-D-16-0065.1.
[16] R. Stuhlmann, A. Rodriguez, S. Tjemkes, J. Grandell, A. Arriaga, J.-.L. Bézy, D. Aminou, P. Bensi, Plans for EUMETSAT's third generation meteosat geostationary satellite programme, Adv. Space Res. 36 (5) (2005) 975–981.
[17] Rudlosky, S.D., and E. Bruning, GLM Gridded product description, 2018. Available in https://vlab.ncep.noaa.gov/.
[18] S.D. Rudlosky, K.S. Virts, Dual geostationary lightning mapper observations, Monthly Weather Rev. 149 (2021) 979–998.
[19] M. Peterson, Removing solar artifacts from geostationary lightning mapper data to document lightning extremes, J. Appl. Remote Sensing 14 (3) (2020), 032402, https://doi.org/10.1117/1.JRS.14.032402.
[20] Goodman, S.J., D. Mach, and K.S. Virts, Lightning: an essential climate variable, in Proc. of the 11th Intl. Conf. on Climate Informatics, Asheville, NC, USA, May 9-13 2022.
[21] K.S. Virts, W.J. Koshak, Mitigation of geostationary lightning mapper geolocation errors, Monthly Weather Rev 37 (2020) 1725–1736.
[22] S.D. Rudlosky, S.J. Goodman, K.S. Virts, E.C. Bruning, Initial geostationary lightning mapper observations, Geophys. Res. Lett. 46 (2019) 1097–1104, https://doi.org/10.1029/2018GL081052.
[23] Montanyà, J., O. van der Velde, N. Pineda and J.A. López-Trujillo, ISS-LIS data analysis based on LMA networks in Europe, EUMETSAT study, 2019, Available in https://www.eumetsat.int/ISS-LIS-data-analysis.
[24] J. Montanyà, J.A. López, C.A. Morales Rodriguez, O.A. van der Velde, F. Fabró, N. Pineda, et al., A simultaneous observation of lightning by ASIM, Colombia-lightning mapping array, GLM, and ISS-LIS, J. Geophys. Res. Atmos. 126 (2021), https://doi.org/10.1029/2020JD033735 e2020JD033735.
[25] Aranguren, D., López, J., Inampués, J., Torres, H., Betz, H.D. (2014), Cloud-to-ground lightning activity in Colombia and the influence of topography. J. Solar Atmos. Solar-Terestria Phys., doi.org/10.1016/j.jastp.2016.08.010.
[26] J. Montanyà, F. Fabró, O. van der Velde, V. March, E.R. Williams, N. Pineda, D. Romero, G. Solà, M. Freijo, Global distribution of winter lightning: a threat to wind turbines and aircraft, Nat. Hazards Earth Syst. Sci. 16 (2016) 1465–1472, https://doi.org/10.5194/nhess-16-1465-2016.
[27] CIGRE WG C4. 409: Lightning protection of wind turbine blades, CIGRE technical brochure, No. 578.
[28] M.M.F. Saba, W. Schulz, T.A. Warner, L.Z.S. Campos, C. Schumann, E.P. Krider, K. L. Cummins, R.E Orville, High-speed video observations of positive lightning flashes to ground, J. Geophys. Res. 115 (2010) D24201, https://doi.org/10.1029/2010JD014330.
[29] A.C.V. Saraiva, M.M.F. Saba, O. Pinto, K.L. Cummins, E.P. Krider, L.Z.S. Campos, A comparative study of negative cloud-to-ground lightning characteristics in São Paulo (Brazil) and Arizona (United States) based on high-speed video observations, J. Geophys. Res. 115 (2010) D11102, https://doi.org/10.1029/2009JD012604.
[30] P.M. Bitzer, Global distribution and properties of continuing current in lightning, J. Geophys.Res. Atmos. 122 (2017) 1033–1041, https://doi.org/10.1002/2016JD025532.
[31] https://www.vaisala.com/en/blog/2020-06/continuing-current-dataset-identifies-lightning-strokes-potential-be-most-destructive, 2020.
[32] CIGRE. WG C4. 410: lightning striking characteristics to very high structures, CIGRE technical brochure, No. 633, 2015.
[33] D. Zhang, K.L. Cummins, Time evolution of satellite-based optical properties in lightning flashes, and its impact on GLM Flash detection, J. Geophys. Res. Atmos. 125 (2020), https://doi.org/10.1029/2019JD032024, 2020e2019JD032024.
[34] S. Visacro, M. Guimaraes, Recent Lightning Measurements and Results At Morro do Cachimbo Station, 23rd Intl. Lightning Detection Conf., Tucson AZ, USA, 2014.
[35] V. Mazur, L.H. Ruhnke, Physical processes during development of upward leaders from tall structures, J. Electrost. 69 (2011) 97–110.
[36] M.M.F. Saba, C. Schumann, T.A. Warner, M.A.S. Ferro, A.R. de Paiva, J. Helsdon Jr, R.E. Orville, Upward lightning flashes characteristics from high-speed videos, J. Geophys. Res. Atmos. (2016) 121, https://doi.org/10.1002/2016JD025137.
[37] D. Wang, N. Takagi, T. Watanabe, H. Sakurano, M. Hashimoto, Observed characteristics of upward leaders that are initiated from a windmill and its

lightning protection tower, Geophys. Res. Lett. 35 (2008) L02803, https://doi.org/10.1029/2007GL032136.
[38] T.A. Warner, J.H. Helsdon Jr., M.J. Bunkers, M.M.F. Saba, R.E Orville, UPLIGHTS: upward lightning triggering study, Bull. Am. Meteorological Soc. 94 (5) (2013) 631–635. Retrieved May 26, 2022, from, https://journals.ametsoc.org/view/journals/bams/94/5/bams-D-11-00252.1.xml.
[39] O.A. van der Velde, J. Montanyà, S. Soula, N. Pineda, J Mlynarczyk, Bidirectional leader development in sprite-producing positive cloud-to-ground flashes: origins and characteristics of positive and negative leaders, J. Geophys. Res. Atmos. 119 (12) (2014), https://doi.org/10.1002/2013JD021291, 755–12,779.
[40] C. Schumann, M.M.F. Saba, T.A. Warner, et al., On the triggering mechanisms of upward lightning, Sci. Rep. 9 (2019) 9576, https://doi.org/10.1038/s41598-019-46122-x.
[41] A.M. Hussein, W. Janischewskyj, J.S. Chang, V. Shostak, W. Chisholm, P. Dzurevych, Z.I. Kawasaki, Simultaneous measurement of lightning parameters for strokes to the Toronto CN tower, J. Geophys. Res.-Atmos. 100 (5) (1995) 8853–8861.
[42] N. Pineda, J. Figueras i Ventura, D. Romero, A. Mostajabi, M. Azadifar, A. Sunjerga, et al., Meteorological aspects of self-initiated upward lightning at the Säntis tower (Switzerland), J. Geophys. Res. Atmos. 124 (2019) 14162–14183, https://doi.org/10.1029/2019JD030834, 2019.
[43] Modelo de Pronóstico de Salidas por Rayos – MPSR. Technical report ISA-INTERCOLOMBIA, 2021.
[44] Peterson, M.J., et al. (2022), New WMO certified megaflash lightning extremes for flash distance (768km) and duration (17.01 s) recorded from space. Bulletin of the American Meteorological Society, doi 10.1175/BAMS-D-21-0254.1.
[45] IEC 62793:2020: Thunderstorm warning systems - protection against lightning.